



HAL
open science

Precipitation kinetics of W₂B₅ in (Ti_{0.4}W_{0.5}Cr_{0.1})B₂ solid solutions

Roland Edith Fotsing, Harald Schmidt, Günter Borchardt, C Schmalzried,
Rainer Telle

► **To cite this version:**

Roland Edith Fotsing, Harald Schmidt, Günter Borchardt, C Schmalzried, Rainer Telle. Precipitation kinetics of W₂B₅ in (Ti_{0.4}W_{0.5}Cr_{0.1})B₂ solid solutions. Philosophical Magazine, 2005, 85 (36), pp.4409-4427. 10.1080/14786430500333323 . hal-00513617

HAL Id: hal-00513617

<https://hal.science/hal-00513617>

Submitted on 1 Sep 2010

HAL is a multi-disciplinary open access archive for the deposit and dissemination of scientific research documents, whether they are published or not. The documents may come from teaching and research institutions in France or abroad, or from public or private research centers.

L'archive ouverte pluridisciplinaire **HAL**, est destinée au dépôt et à la diffusion de documents scientifiques de niveau recherche, publiés ou non, émanant des établissements d'enseignement et de recherche français ou étrangers, des laboratoires publics ou privés.



Precipitation kinetics of W2B5 in (Ti0.4W0.5Cr0.1)B2 solid solutions

Journal:	<i>Philosophical Magazine & Philosophical Magazine Letters</i>
Manuscript ID:	TPHM-05-Jul-0337.R1
Journal Selection:	Philosophical Magazine
Date Submitted by the Author:	26-Aug-2005
Complete List of Authors:	Fotsing, Roland; TU Clausthal, IMET Schmidt, Harald; TU Clausthal, IMET Borchardt, Günter; TU Clausthal, IMET Schmalzried, C; RWTH Aachen, Institut für Gesteinshüttenkunde Telle, Rainer; RWTH Aachen
Keywords:	transition-metal compounds, precipitation, kinetics, borides
Keywords (user supplied):	JMAK model



Precipitation kinetics of W_2B_5 in $(Ti_{0.4}W_{0.5}Cr_{0.1})B_2$ solid solutions

E. R. FOTSING†, H. SCHMIDT*†, G. BORCHARDT†, C. SCHMALZRIED‡, and
R. TELLE‡

† Fakultät für Natur- und Materialwissenschaften, AG Thermochemie und Mikrokinetik,
TU Clausthal, Robert-Koch-Str.42, D-38678 Clausthal-Zellerfeld, Germany

‡ Institut für Gesteinshüttenkunde, RWTH Aachen, Mauerstr.5, 52064 Aachen, Germany

* Corresponding author:

Dr. Harald Schmidt
TU Clausthal
IMET/AG Thermochemie und Mikrokinetik
Robert-Koch-Str. 42
D-38678 Clausthal-Zellerfeld
Germany
Tel: +49/5323/72-2094
Fax: +49/5323/72-3184
E-mail: harald.schmidt@tu-clausthal.de

1
2
3 The isothermal precipitation kinetics of W_2B_5 secondary phase from supersaturated
4 polycrystalline $(Ti_{0.4}W_{0.5}Cr_{0.1})B_2$ solid solutions were investigated with X-ray diffractometry
5 (XRD) and secondary electron microscopy (SEM) in the temperature range between 1500 and
6 1700 °C. The precipitate formation is described by a modified Johnson-Mehl-Avrami-
7 Kolmogorov (JMAK) model, where W_2B_5 particles nucleate preferably at grain boundaries
8 and subsequently grow into the volume by a two-dimensional process controlled by volume
9 diffusion of the transition metals. Numerical calculations are used to quantitatively describe
10 the time dependence of the precipitated fraction and to determine a differential JMAK
11 exponent, n_{diff} , which gives information on nucleation and growth modes. n_{diff} decreases
12 during the precipitation process from 2 to about 0.8 for all temperatures investigated. The first
13 limit corresponds to the classical JMAK model (two-dimensional diffusional growth and
14 constant nucleation rate) and the decrease of n_{diff} is the consequence of an impingement of the
15 nucleating and growing particles in the late stages of the process. Nucleation and growth rates
16 are determined as a function of reciprocal temperature, where the first quantity shows a non-
17 monotonic behaviour with a maximum at about 1650 °C and the second quantity exhibits an
18 Arrhenius behaviour with an activation enthalpy of 3.6 eV. Herefrom it can be concluded that
19 the overall precipitate formation is dominated by the kinetics of atomic motion at low
20 temperatures and by the thermodynamics of nucleation at high temperatures.
21
22
23
24
25
26
27
28
29
30
31
32
33
34
35
36
37
38
39
40
41
42
43
44
45
46
47
48
49
50
51
52
53
54
55

56 *Keywords:* Precipitation kinetics; transition metal diborides; heterogeneous nucleation; JMAK
57
58 model
59
60

1. Introduction

Considerable interest in transition metal diboride ceramics is fostered by attractive materials properties, such as a high melting point, a high hardness, and a good electrical and thermal conductivity [1,2]. Besides these qualities, many of these diborides are distinguished by large temperature dependent homogeneity ranges which are bordered by miscibility gaps as demonstrated for the system $\text{TiB}_2\text{-WB}_2\text{-CrB}_2$ [3,4]. Annealing of homogeneous solid solutions at temperature below the homogenization temperature leads to the precipitation of elongated particles with a high aspect ratio [3,5,6]. These elongated precipitates are expected to improve the toughness and creep resistance and are the basis of the development of in-situ reinforced boride ceramics [5]. To achieve this purpose, it is important to understand the formation of the precipitates and the underlying kinetic processes, which are governed by long range diffusion. Up to now, no systematic studies on the precipitation kinetics of these materials were carried out. However, investigations on the self-diffusion of Ti and Cr suggest that the growth of the precipitates is controlled by bulk diffusion of the transition metals [7].

In this study we used X-ray diffractometry (XRD) and secondary electron microscopy (SEM) to monitor the time evolution of the volume fraction of the precipitated phase and of the average particle diameter as a function of annealing time. A modified model, based on the theory of Johnson, Mehl, Avrami, and Kolmogorov (JMAK theory), was used to describe the precipitation kinetics. As a model system, ceramics with the nominal composition $(\text{Ti}_{0.4}\text{W}_{0.5}\text{Cr}_{0.1})\text{B}_2$ were used for the present investigations, which show good conditions for the growth of reinforcing platelets [6].

2. Experimental details

Samples with nominal composition $(\text{Ti}_{0.4}\text{W}_{0.5}\text{Cr}_{0.1})\text{B}_2$ were produced by reaction sintering of TiB_2 , WB_2 , and CrB_2 powders (H. C. Starck, Germany) containing less than 1 wt.-% of

1
2
3 impurities (C, Fe, N, O). The reaction sintering process was carried out in a uniaxial graphite
4 hot press at a pressure of 60 MPa and at a temperature of 1800 °C for 30 min in argon
5 atmosphere. Afterwards, the specimens were homogenized at 2000 °C for 8 hours at ambient
6 pressure in argon. For the precipitation experiments, slabs of 8 x 8 x 2 mm³ were cut from the
7 interior of the hot pressed samples, polished with diamond paste and cleaned with ethanol.
8 The samples were isothermally annealed at temperatures between 1500 °C and 1700 °C in an
9 argon atmosphere at ambient pressure for times between 0.5 h and 40 h to observe
10 precipitation. In order to avoid the formation of oxide layers during annealing, two samples
11 were placed on each other with the polished surface, mounted in a crucible and were
12 surrounded by fine powder of TiB₂. To ensure isothermal annealing conditions, very short
13 heating and cooling times of the samples were realized with a special mechanical transfer unit
14 whereby the samples can be placed in the hot zone of the furnace within 5 minutes. In order to
15 observe the kinetics of precipitation the following procedure was applied: first, the solid
16 solutions were isothermally annealed at a distinct temperature for a given time t_a . Then the
17 material was characterized by X-ray diffractometry (XRD), scanning electron microscopy
18 (SEM), and energy dispersive X-ray analysis (EDX), and afterwards annealed again. This
19 procedure was repeated until full precipitation was achieved.
20
21
22
23
24
25
26
27
28
29
30
31
32
33
34
35
36
37
38
39
40
41
42

43 The investigations with XRD were carried out with a SIEMENS D5000/Kristalloflex
44 diffractometer in the $\theta/2\theta$ mode using CoK_α radiation (40 kV, 40 nA) on bulk ceramics. An
45 adjustable sample holder was used to position the sample surface reproducibly in the
46 incidence plane of the X-rays. The SEM studies were made on a CamScan 44 apparatus with
47 a tungsten cathode. The composition of the matrix the and precipitates was investigated by
48 electron beam micro analysis (Cameca SX-100) with an EDX detector operating at an
49 acceleration voltage of 20 kV for a penetration depth of 1-3 μm .
50
51
52
53
54
55
56
57
58
59
60

3. Results and discussion

3.1 Experimental results

Fig. 1(a) shows XRD diagrams of a sample after homogenisation at 2000 °C and after additional thermal annealing at 1575 °C. For the as-homogenized sample all peaks are characteristic for the TiB_2 structure (space group: $P6/mmm$) [6], indicating the presence of a $(\text{Ti, Cr, W})\text{B}_2$ solid solution. With EDX, a transition metal composition of 40.0 ± 2.0 at. % of Ti, 49.5 ± 2.5 at. % of W, and 10.5 ± 1.0 at.% of Cr is detected. Thus, the measured concentrations correspond to an overall sample composition of $(\text{Ti}_{0.4}\text{W}_{0.5}\text{Cr}_{0.1})\text{B}_2$. In contrast, for the precipitation annealed sample new peaks appear, which correspond to a tungsten rich precipitate phase with W_2B_5 structure (space group: $P6_3/mmc$) [6] and a chemical composition of $(\text{Ti}_{0.1}\text{W}_{0.8}\text{Cr}_{0.1})\text{B}_{2+x}$. The boron concentration of compounds crystallizing in the W_2B_5 structure is not yet determined exactly up to now, however, literature data indicate values between $-0.15 < x < 0.27$ [6]. The strongest line of the precipitated phase corresponds to the (004) reflection of the hexagonal structure. This line is used for monitoring the precipitation process as a function of annealing time as explained in the last section. The variation of this peak during annealing is illustrated in Fig. 1(b). Further analysis was carried out assuming that the precipitated volume of the precipitated phase, $V(t)$, is proportional to the integrated intensity of the (004) X-ray peak, $J(t)$. The volume fraction $X(t) = J(t)/J^{max}$ of precipitated phase at an annealing time t can now be calculated with J^{max} as the corresponding value for complete precipitation. Exemplary results determined at various temperatures are given in Fig. 2. Data analysis is realized with the models developed in Appendix A.

[Insert figure 1 about here]

1
2
3
4
5
6 [Insert figure 2 about here]
7
8
9

10
11 In Fig. 3 (a) - (d) SEM micrographs are displayed, which illustrate the development of the
12 microstructure during the precipitation process. The images show a region of the sample
13 surface, where W_2B_5 particles are precipitated from the supersaturated $(Ti_{0.4}W_{0.5}Cr_{0.1})B_2$
14 matrix. From the SEM micrographs it can be concluded that (i) nucleation takes place
15 predominantly at grain boundaries and (ii) the growth of the nucleated particles proceeds into
16 the volume of the grain. As illustrated in Refs. [3,5,7] the precipitated phase has the form of
17 platelets with a high aspect ratio. This is also visible in Fig. 3, where a platelet-like particle is
18 observed which grows perpendicular to the surface as a function of annealing time. Platelets
19 with dimensions of up to 15 μm and a maximum thickness of only 1 μm are observed on
20 various micrographs. This morphology indicates a two-dimensional growth of precipitated
21 particles.
22
23
24
25
26
27
28
29
30
31
32
33
34
35
36
37
38
39

40 [Insert figure 3 about here]
41
42
43
44

45 Using an image analysis software (ANALYSIS 5.0), the precipitate dimension in growth
46 direction, d , was measured as a function of annealing time for various precipitates. Examples
47 at different temperatures are shown in Fig. 4, where d^2 is plotted against annealing time.
48
49 Diffusion controlled growth is expected in the present materials, because long range re-
50 arrangement processes of atoms in the matrix are necessary in order to form W_2B_5
51 precipitates. The precipitate growth process may be visualized in the following way: W atoms
52 diffuse along a gradient of the chemical potential from the matrix to the precipitate, where
53 they are incorporated and at the same time Cr and Ti atoms diffuse away from the precipitate
54
55
56
57
58
59
60

1
2
3 region to the matrix. This might take place in the volume of the material or along grain
4
5 boundaries. The data in Fig. 4 are fitted by equation (A.8) (see Appendix) according to a
6
7 diffusion controlled growth process. Averaging over several particle growth curves gives a
8
9 value for an effective diffusivity D_e which is plotted in Fig. 10 as a function of reciprocal
10
11 temperature. Further discussion is carried out in section 3.4.
12
13

14
15
16 [Insert figure 4 about here]
17
18
19
20

21
22 The SEM micrographs revealed also that the distance between particles nucleated at grain
23
24 boundaries, d_c , is between 1 and 10 μm (see Fig. 3). Herefrom it is possible to assess the
25
26 contribution of grain boundary diffusion to the growth process. We define a volume $V_c = a A_c$
27
28 around a nucleated particle in a grain boundary, where atoms of the supersaturated matrix
29
30 may contribute to the growth of this special particle by diffusion (see Fig. 5). Atoms outside
31
32 this volume contribute to the growth of neighbouring particles. Using, $a \approx 0.1 \text{ nm}$ as the
33
34 approximate width of a grain boundary and $A_c = 1 - 100 \mu\text{m}^2$, a value of $V_c = 10^{-22} - 10^{-20} \text{ m}^3$ is
35
36 obtained for the volume of matrix material which may contribute to the growth of the
37
38 precipitated phase only by grain boundary diffusion. Considering a spherical growth of the
39
40 precipitates in the very first stages of the precipitation process, we obtain a maximum radius
41
42 of $r_{\text{max}} \approx 3/(4 \pi) V_c^{1/3} \approx 10 - 50 \text{ nm}$ for a particle that grows after nucleation only due to matter
43
44 transport in the grain boundaries, where the particle densities of the matrix and the precipitate
45
46 are assumed to be approximately the same. This radius is negligible compared to the average
47
48 size of the particle after complete precipitation of 5 - 15 μm . This result suggests that if there
49
50 is a contribution of grain boundary diffusion to growth, this contribution is limited to the early
51
52 stages of the growth process after nucleation. A particle radius of about 10 - 50 nm is much
53
54 too small to be observed with SEM and is consequently also not accounted for during further
55
56 analysis. For the nucleated particles to grow to larger radii a transport through the grain
57
58
59
60

1
2
3 volume is necessary, which becomes the rate limiting process. As a result from these
4
5 considerations, we can assume that the diffusion in grain boundaries does not significantly
6
7 contribute to the observed growth process.
8
9

10
11
12
13
14 [Insert figure 5 about here]
15
16
17

18
19
20 As a result from the experimental observations with XRD, SEM, and EDX it can be
21
22 concluded that during precipitation annealing of homogeneous $(\text{Ti}_{0.4}\text{W}_{0.5}\text{Cr}_{0.1})\text{B}_2$ ceramics,
23
24 W_2B_5 precipitates nucleate predominantly at grain boundaries and grow into the grain volume
25
26 in a two-dimensional process. Generally, the evolution of the volume fraction of a precipitated
27
28 phase within a homogeneous matrix during annealing can be described by the so called
29
30 JMAK model [8-10] (see Appendix A.1). Using equation (A.5), the experimental data in Fig.
31
32 2 can be least-squares fitted, which results in straight lines if $\ln(-\ln(1-X))$ is plotted as function
33
34 of $\ln t$ for each annealing temperature (JMAK plot). This means that the experimental data can
35
36 be described very well with the JMAK model. JMAK exponents between $n = 1.5$ and 1.8 are
37
38 obtained, which would correspond to a two-dimensional growth with a varying, e. g. slightly
39
40 decreasing, nucleation rate. However, the JMAK model is not in accordance with the
41
42 observation that nucleation occurs predominantly at grain boundaries, which is not considered
43
44 in the derivation of the original JMAK model.
45
46
47
48
49

50 51 **3.2 Numerical Calculations according to the GBJMAK model** 52

53
54 In Appendix A.2, a modified JMAK model based on Refs. [12-14] is developed and
55
56 adapted to the present system, which includes nucleation at grain boundaries (GBJMAK
57
58 model) and two-dimensional diffusion controlled growth of disk-like particles in volume.
59
60 Equations (A.7), (A.8), (A.13), and (A.14) allow to determine the volume fraction of

precipitated particles as a function of time, $X(t)$. The present equations were solved numerically using the MATHEMATICA computer software package (Version 5.0). As input parameter a grain boundary density of $\rho_B = (\text{grain boundary area} / \text{grain boundary volume}) \approx 3 \times 10^5 \text{ m}^{-1}$ is used, which is calculated using an average grain size of about $20 \mu\text{m}$. The thickness of the precipitates is about $h = 1 \mu\text{m}$. It appears that only three free parameters are determinant for the calculation, namely the effective diffusivity, D_e , the nucleation rate, I_B , which is assumed to be constant, and the number of pre-existing nuclei at the grain boundary, N_{B0} . **The total** number of nuclei which are formed by continuous nucleation can be calculated by

$$N_B = \int_0^{\infty} I_B (1 - X(t)) dt. \quad (1)$$

In order to illustrate the influence of I_B and N_{B0} on the time dependence of the precipitated fraction, X , calculations were carried out for a constant effective diffusivity of $D_e = 1.2 \times 10^{-15} \text{ m}^2 \text{ s}^{-1}$, which are shown in Fig. 6(a). Three different cases are distinguished: (I) $I_B = 2 \times 10^7 \text{ m}^{-2} \text{ s}^{-1}$, $N_{B0} = 0$, (II) $I_B = 2 \times 10^7 \text{ m}^{-2} \text{ s}^{-1}$, $N_{B0} = 3 \times 10^{10} \text{ m}^{-2}$ ($N_B > N_{B0}$), and (III) $I_B = 2 \times 10^7 \text{ m}^{-2} \text{ s}^{-1}$, $N_{B0} = 2.5 \times 10^{11} \text{ m}^{-2}$ ($N_B \approx N_{B0}$). For all three cases, the profiles exhibit a non-linear behaviour which indicates a change in the growth dimensionality and in the nucleation mode during precipitation, in contrast to the JMAK model (see Fig. 2). In Fig. 6(b) the quantity

$$n_{diff} = \frac{\partial \ln(-\ln(1 - X))}{\partial \ln(t)}. \quad (2)$$

is plotted, which is termed the differential JMAK exponent and which is a measure for this change. This exponent is constant in case of the original JMAK model, however, in case of the present GBJMAK model n_{diff} is changing with the proceeding transformation. For case (I), where N_{B0} is zero, n_{diff} decreases monotonically from a starting value of 2 in the early stages of the process, to about $n_{diff} = 0.5$ at the end of the transformation process. The first value

1
2
3 represents an exponent as obtained from the classical JMAK theory for a two-dimensional
4 diffusion controlled growth with constant nucleation rate (however in the volume). The
5 decrease of the exponent during precipitation indicates an overlapping of the nucleation and
6 diffusion zones of the particles. Consequently, the precipitation rate slows down (deviation
7 from linear behaviour) and the value for the JMAK exponent falls down to $n_{\text{diff}} = 0.5$, which
8 correspond to a one-dimensional growth from pre-existing nuclei. At this stage no more new
9 nuclei can be formed at grain boundaries due to impingement and only the already existing
10 nuclei may grow. Note that an approximately constant value of about $n_{\text{diff}} = 2$ is maintained
11 until about 50 % of the transformation ($\ln t = 8.46$) is completed. For case (II), for the same
12 nucleation rate as in case (I), an additional concentration of pre-existing nuclei is present.
13 However, the condition $N_B > N_{B0}$ is valid. As shown in Fig. 6(b), the differential JMAK
14 exponent shows a strongly non-monotonic behaviour. At the beginning of the transformation
15 process it is close to $n_{\text{diff}} = 1$, due to the presence of pre-existing nuclei. During further
16 transformation, n_{diff} increases due to the additional formation of nuclei and reaches a
17 maximum when about 50 % of the transformation is completed. At the end of the process n_{diff}
18 drops to 0.5. Finally for case (III), where $N_B \approx N_{B0}$ is valid, the differential JMAK exponent is
19 close to 1 at the beginning and changes only slightly during the whole precipitation process,
20 which means that the pre-existing nuclei dominate the transformation. The case where no
21 new nuclei are formed during the precipitation process ($I_B = 0$) is nearly identical to case (III).

22
23
24
25
26
27
28
29
30
31
32
33
34
35
36
37
38
39
40
41
42
43
44
45
46
47
48
49
50
51 [Insert figure 6 about here]
52
53
54
55

56 In order to illustrate the development of the precipitated fraction and of the differential
57 JMAK exponent with increasing nucleation rate, calculations of these quantities are displayed
58 in Fig. 7(a) and (b) for $N_{0B} = 0$. It is obvious that for a very small nucleation rate (case (I)) an
59
60

1
2
3 approximate straight line results with an almost constant value of n_{diff} between 1.8 and 2 until
4
5 70 % of the precipitates are formed. This corresponds to a two-dimensional growth with
6
7 continuous nucleation during nearly the whole transformation process. Only at the very end of
8
9 the transformation n_{diff} drops to 0.5. With increasing nucleation rates, n_{diff} decreases
10
11 significantly during the transformation, resulting in non-linear curves in Fig. 7(a). For case
12
13 (IV) in Fig. 7, a value of $n_{\text{diff}} = 0.5$ is obtained after only 50 % of the volume is precipitated.
14
15 This is the consequence of an impingement of the growing particles already at the beginning
16
17 of the precipitation process due to the high nucleation rate. Numerous and densely packed
18
19 nuclei that encumber each other force the particles to grow in one dimension only,
20
21 perpendicular to the grain boundary plane. These results show that with increasing nucleation
22
23 rate a crossover occurs from a two-dimensional growth process with continuous nucleation to
24
25 a one-dimensional growth process with strong impingement in the very early stages.
26
27
28
29
30
31
32

33 [Insert figure 7 about here]
34
35
36
37

38 **3.3 Comparison between experiments and the GBJMAK model**

39
40
41 For an analysis of the experimental data, it is important to know which range of the calculated
42
43 precipitation curves can be attained experimentally. It became obvious from the experiments
44
45 that a precipitated fraction, X , in the range between 0.05 and 0.95 can be measured with an
46
47 adequate accuracy. Fig. 6(a) shows that in this range the calculated curves can be
48
49 approximated roughly by a straight line, meaning that a change of the differential JMAK
50
51 exponent during precipitation is not necessarily observable in the experiments.
52
53
54
55

56 In order to find out which of the two quantities N_{0B} and I_B is determinant for the observed
57
58 precipitation process, the experimental data at a temperature of 1500 °C are compared
59
60 exemplarily to simulations based on the GBJMAK model in Fig. 8. To achieve this, one
parameter is set to a certain value and the other is obtained by least-squares fitting in such a

way that the experimental data are described at their best. The effective diffusivity is set to a constant value of $D_e = 1.2 \times 10^{-15} \text{ m}^2 \text{ s}^{-1}$, as extracted from the growth rates in Fig. 4. As can be seen from Fig. 8, the best accordance between experimental data and calculations is obtained for $N_{0B} \approx 0$ ($N_B \gg N_{0B}$). This means that the precipitation kinetics in the present diboride compounds can be described by a continuous nucleation of particles at grain boundaries and a consecutive growth into the volume. The precipitated fraction is then given by (see Appendix A)

$$X(t) = 1 - \exp\left(-\rho_B 2 \int_0^{R(t,0)} \left(1 - \exp\left(-\frac{4hI_B}{3D_e}(R^2 - y^2)^{3/2}\right)\right) dy\right). \quad (3)$$

All experimental data in the temperature range between 1500 and 1700 °C were fitted with a constant value of D_e as extracted from the particle growth rates (Fig. 10) and with I_B as a fit parameter. Examples for the resulting curves are plotted in Fig. 9. In Fig. 9(a) the transformed volume fraction and in Fig. 9(b) the differential JMAK exponent as calculated from the fit curves are given. The experimentally determined precipitated fraction is described very well by the model within error limits. The curves exhibit only a small non-linearity as a consequence of the heterogeneous nucleation at grain boundaries, instead of being straight lines as expected from the classical JMAK model (Fig. 2). The differential JMAK exponent does not remain constant and decreases progressively from $n_{\text{diff}} = 2$ to 0.8 during the transformation at all temperatures. The first limit corresponds to the classical JMAK model and the second value is the consequence of the impingement of the growing particles in the late stages of the process. A clearly one-dimensional growth corresponding to $n_{\text{diff}} = 0.5$ is not observed until the completion of the experimentally observable precipitation process.

[Insert figure 8 about here]

[Insert figure 9 about here]

3.4 Temperature dependence of nucleation, growth, and precipitation rates

From the effective diffusivities D_e , which were obtained from the growth of the crystallites in Sec. 3.1, the bulk diffusivities, D_V , are calculated using equation (A.8) and $\gamma = 0.3$ (from XRD measurements). The results are plotted in Fig. 10 as a function of reciprocal temperature. The data obey an Arrhenius law according to

$$D_V = D_0 \exp\left(-\frac{\Delta H^g}{k_B T}\right), \quad (4)$$

where $D_0 = 3.8 \cdot 10^{-5} \text{ m}^2 \text{ s}^{-1}$ is the pre-exponential factor and $\Delta H^g = (3.6 \pm 0.9) \text{ eV}$ is the activation enthalpy of crystallite growth, which can be identified with the activation enthalpy of transition metal self-diffusion, ΔH^D . Also shown are tracer bulk diffusivities of Ti in the same $(\text{Ti}_{0.4}\text{W}_{0.5}\text{Cr}_{0.1})\text{B}_2$ material in the as-homogenized state, as measured in Ref. [15]. Ti is found to be the slowest diffusing species in this materials and should consequently be growth-limiting. The activation enthalpy of Ti tracer diffusion of $\Delta H_{\text{Ti}} = (3.9 \pm 0.5) \text{ eV}$ is identical with the activation enthalpy of particle growth within estimated errors. However, the tracer diffusivities, extrapolated to higher temperatures, are lower by about three orders of magnitude. Note that the Cr tracer diffusivities, which are the fastest transition metal species in these materials, are only one order of magnitude higher than the Ti diffusivities [15]. It is also shown in Ref. [15] that the tracer diffusivities do not change significantly during the precipitation process. Thus, the difference between the diffusivities obtained from growth rates and the tracer diffusivities is unexplained at the moment. However, due to the fact that precipitate growth should be governed by chemical diffusion in a gradient of the chemical potential and not by tracer diffusion, interdiffusion measurements are necessary for a correct interpretation of the data. A further possible reason for the discrepancy between the tracer diffusivities and the diffusivities obtained from growth data might be the influence of dislocations or stacking faults, which are present in the diboride compounds [5]. **However, the**

1
2
3 tracer diffusion measurements in Ref. [15] were not sensitive enough to detect such
4
5 accelerated diffusion along these defects.
6
7
8
9

10 [Insert figure 10 about here]
11
12
13
14

15 Using the diffusivities (or the linear extrapolation of the diffusivities) as obtained from the
16 growth data in Fig. 10 as input parameters for the calculations, the grain boundary nucleation
17 rates, I_B , can be determined as a function of temperature, as shown in Fig. 11. The nucleation
18 rates exhibit a non-monotonic behaviour, where $\log I_B$ increases with reciprocal temperature
19 between 1700 and 1650 °C, has a maximum around 1650 °C, and decreases linearly for lower
20 temperatures. Using the linear extrapolation of the Ti tracer diffusivities as input parameters
21 for the calculations, very high nucleation rates are necessary to compensate the slower
22 growth. This, however, leads to a completely unsatisfying description of the experimental data
23 by the numerical calculations, because strong impingement occurs during the early stages of
24 precipitation.
25
26
27
28
29
30
31
32
33
34
35
36
37
38
39

40 According to the theory of heterogeneous nucleation, the nucleation rate is given by [16]
41

$$I_B = I_0 \exp\left(-\frac{\Delta H^I + \Delta G^*}{k_B T}\right) \quad (5)$$

42 where ΔG^* is the Gibbs free energy change for nucleus formation at grain boundaries, ΔH^I is
43 the enthalpy for the transfer of an atom across the particle interface and its subsequent
44 incorporation into the lattice of the precipitate, which can be approximately set as the
45 activation enthalpy of self-diffusion, $\Delta H^I \approx \Delta H^D$, and I_0 is a pre-exponential factor. ΔG^* can be
46 approximated by [16]
47
48
49
50
51
52
53
54
55
56
57
58
59
60

$$\Delta G^* = \frac{A}{(T - T^*)^2} \quad (6)$$

1
2
3 where $\Delta T = T^* - T$ is the undercooling of the material compared to a temperature T^* where
4 matrix phase and precipitate phase are in equilibrium. The influence of this term leads to the
5 observed non-linear behaviour of the nucleation rates in the Arrhenius plot of Fig. 11. The
6 nucleation rates in Fig. 11 are fitted to equation (5) and (6) with A , I_0 , and T^* as fit parameters
7 and $\Delta H^I = \Delta H^S = 3.6$ eV (solid line in Fig.11). An equilibrium temperature of $T^* = (1750 \pm$
8 $50)$ °C is obtained, which means that at temperatures above T^* no precipitates are formed. For
9 $T \ll T^*$, ΔG^* reaches a constant value of 4×10^{-4} eV, meaning that nucleation is controlled by
10 the transfer of an atom across the phase boundary between precipitate and matrix with an
11 activation enthalpy $\Delta H^I = 3.6$ eV. In contrast for $T^* < T < T^{\max}$, ΔG^* becomes the dominating
12 term which results in a decrease of the nucleation rate with increasing temperature and can be
13 explained by the fact that ΔT becomes very small and the driving force of nucleation
14 approaches zero. It should also be noted that a fit of the experimental data in Fig. 11 to
15 equation (5) with $\Delta H^I = 0$ does not give a reasonable description of the data, which means that
16 the atomic transfer across the phase boundary is an important factor determining nucleation.
17
18
19
20
21
22
23
24
25
26
27
28
29
30
31
32
33
34
35

36
37 [Insert figure 11 about here]
38
39
40
41

42 Also shown in Fig. 11 are the overall rate constants of precipitation, k_p , which are
43 determined from the experimental data in Fig. 9(a) using a characteristic time constant $t^* =$
44 k_p^{-1} which is defined as $X(t^*) = 0.632$ in analogy to a JMAK type of transformation. As is
45 obvious from Fig. 11, a non-monotonic behaviour similar to the temperature dependence of
46 the nucleation rate is observed. This is due to a combined influence of the Arrhenius
47 behaviour of the diffusivity (which governs the growth kinetics and the transfer of atoms
48 across the phase boundary) and of the Gibbs free energy change of nucleus formation (which
49 reflects the influence of thermodynamics). A description of the temperature dependence of k_p
50 is obtained by inserting equations (4) and (5) into equation (3). For $X = 0.632$ an implicit
51
52
53
54
55
56
57
58
59
60

1
2
3 equation for $k_p(T)$ results with I_0 , T^* , A , D_0 , and ΔH^g as parameters known from fitting the
4
5 temperature dependence of the nucleation and growth rates. Numerical calculations lead to the
6
7 curve which is shown in Fig. 11 as a dashed line.
8
9

10 11 **4. Conclusion** 12

13
14 From the present investigations on the isothermal precipitation kinetics of W_2B_5 in
15
16 supersaturated $(Ti_{0.4}W_{0.5}Cr_{0.1})B_2$ solid solutions between 1500 and 1700 °C the following
17
18 conclusions can be drawn:
19
20

- 21
22 • XRD and SEM measurements show the formation of plate-like precipitates, which
23
24 nucleate preferably at grain boundaries and grow into the interior of the matrix grains
25
26 according to a two-dimensional diffusion controlled growth process.
27
28
- 29
30 • The experimentally determined precipitate fraction as a function of annealing time can be
31
32 described by a modified JMAK model which takes into account nucleation at grain
33
34 boundaries.
35
36
- 37
38 • It was found that during the precipitation process a crossover occurs from a two-
39
40 dimensional growth process with continuous nucleation to a one-dimensional growth
41
42 process from already formed nuclei, while impingement of the growing nuclei prevent
43
44 further nucleation at grain boundaries.
45
46
- 47
48 • Effective diffusivities are determined from the growth of nucleated particles, which are
49
50 about three order of magnitude higher than literature data on Ti and Cr tracer diffusivities.
51
52 However, both quantities show an Arrhenius behaviour with an activation enthalpy of
53
54 about 3.6 eV.
55
56
- 57
58 • The determined nucleation rates and precipitation rates show a non-monotonic behaviour
59
60 as a function of reciprocal temperature with a maximum at about 1650 °C.

- The overall rate of precipitate formation is determined by the kinetics of atomic motion at low temperatures and by the thermodynamics of nucleation at high temperatures.

Acknowledgements

The authors would like to thank E. Ebeling for the ceramographic preparation of the sample surfaces and B. Mühlhan and S. Lenk for their assistance in SEM analysis. The authors are also grateful to P. Klein for helpful discussions in relation to the numerical calculations. This work was supported by the Deutsche Forschungsgemeinschaft (DFG).

Appendix A: Theoretical background

A.1 The JMAK model

The evolution of the volume fraction of a precipitated phase within a homogeneous matrix during annealing at a temperature T can be described by the JMAK equation [8-10] by

$$X(T, t) = 1 - \exp(-X_e(T, t)), \quad (\text{A.1})$$

where $X_e(T, t)$ is the extended volume fraction, which is obtained by assuming that all particles grow unrestrictedly. In order to model the present precipitation process, we consider a disc of radius R with a thickness of $h < R$ and a radial growth of the nucleated particles. In case of a two-dimensional diffusion controlled growth, $X_e(T, t)$ is related to the time and temperature dependent nucleation rate $I(T, t)$ and an effective diffusivity $D(Tt)$ by

$$X_e(T, t) = \pi h \int_0^t I(T, \tau) D_e(T)(t - \tau) d\tau. \quad (\text{A.2})$$

1
2
3 Assuming a constant nucleation rate, I , during the transformation the fraction of precipitated
4
5 phase can be written as
6
7

$$X = 1 - \exp(-0.5\pi h I D_e t^2). \quad (\text{A.3})$$

8
9
10 For a transformation process starting from pre-existing nuclei with no appreciable nucleation
11
12 during the phase transformation, we obtain
13
14

$$X = 1 - \exp(-\pi h N_0 D_e t), \quad (\text{A.4})$$

15
16
17 where N_0 is the density of the pre-existing nuclei. Often, an effective rate constant, k_p , is
18
19 defined, which is a function of the nucleation rate and of the diffusivity, leading to the well-
20
21 known JMAK equation derived by Johnson, Mehl, Avrami, and Kolmogorov [8-10]
22
23
24
25
26
27

$$X = 1 - \exp(- (k_p t)^n), \quad (\text{A.5})$$

28
29
30 where n is the JMAK exponent giving information on the dimensionality of the growth
31
32 process and on the influence of the nucleation. Following the above description, an exponent
33
34 of $n = 2$ is obtained for a constant nucleation rate and of $n = 1$ for a growth from pre-existing
35
36 nuclei.
37
38
39
40

41 42 **A.2 The GBJMAK model**

43
44
45 In order to correctly describe the experimental data obtained in this study, a modified JMAK
46
47 model is developed which includes nucleation at grain boundaries and is termed GBJMAK
48
49 model (GB: grain boundary). It is based on the classical JMAK theory with extension to
50
51 heterogeneous nucleation at grain boundaries as first derived by Cahn [14,15]. Recently,
52
53 Bakai et al. [16] developed an expression for the transformed volume fraction, by taking into
54
55 account the contributions of grain boundaries
56
57
58
59
60

$$X(t) = 1 - \exp(- (1 - a\rho_B) Y_V(t) - \rho_B Y_B(t)), \quad (\text{A.6})$$

where Y_V and Y_B are the extended volume fractions of the precipitates formed in the bulk and in the grain boundaries, respectively, ρ_B is the grain boundary density, and a is the width of the grain boundary layer. Since in the present case nucleation takes place preferably at grain boundaries we get

$$X(t) \approx 1 - \exp(-\rho_B Y_B(t)). \quad (\text{A.7})$$

A radial growth of the nucleated particles is assumed to take place approximately perpendicular to the grain boundary plane. Here, $R(t, \tau)$ is the radius of a disk-like precipitate at time t , which was formed at time τ at a grain boundary plane. Thus, R is given by

$$R^2 = D_e (t - \tau) = 2 \frac{C_m - C_s}{C_p - C_s} D_V (t - \tau) \quad (\text{A.8})$$

where D_e is an effective diffusivity, D_V is the diffusivity of the slowest mobile element in the volume. and C_m , C_s , and C_p are the concentrations of the diffusing element in the matrix, at the precipitate-matrix interface, and in the precipitate. The ratio $\gamma = (C_m - C_s)/(C_p - C_s)$ in equation (A.8) corresponds to the fraction of precipitated phase at the end of the process [11]. In order to determine the volume fraction occupied by particles nucleated at grain boundaries, the concept of Cahn for the derivation of rate laws for transformations in which a new phase nucleates at grain boundaries was used [14,15]. Consider a plane parallel to a given grain boundary, which is situated at a distance y from it. This plane intersects nucleated particles with a radius $R(t, \tau) > y$ and the intersection area for a given disc-like nucleus is $2h(R^2(t, \tau) - y^2)^{1/2}$. The total intersection area of all nuclei is then obtained by

$$Y_B^e(y, t) = 2hN_{OB} (R^2(t, 0) - y^2)^{1/2} + 2h \int_0^{t_m(y)} I_B(\tau) (R^2(t, \tau) - y^2)^{1/2} d\tau, \quad (\text{A.9})$$

where N_{0B} is the density of pre-existing nuclei at grain boundaries, I_B is the nucleation rate at grain boundaries, and $t_m(y)$ is defined as $R(t, t_m) = y$. Since the intersections are randomly distributed, the relation [16]

$$Y_B(y, t) = 1 - \exp(-Y_B^e(y, t)). \quad (\text{A.10})$$

can be used. The total contribution of grain boundaries to the precipitated volume fraction is then defined by

$$Y_B(t) = 2 \int_0^{\infty} 1 - \exp(-Y_B^e(y, t)) dy. \quad (\text{A.11})$$

Using

$$d\tau = -\frac{R}{\gamma D_V} dR \quad (\text{A.12})$$

equation (A.9) can be substituted and integrated under the assumption that the nucleation rate is time independent, $I_B(t) = I_B$, and that the critical radius of the precipitate is approximately zero. Equations (A.9), (A.10), and (A.11) can now be transformed into

$$Y_B(t) = 2 \int_0^{R(t,0)} 1 - \exp(-Z(R(t,0), y)) dy, \quad (\text{A.13})$$

where $R(t, 0)$ is the maximum precipitate radius and the function $Z(R, y)$ has the form

$$Z(R, y) = 2N_{0B}h(R^2 - y^2)^{1/2} + \frac{2hI_B}{3\gamma D_V}(R^2 - y^2)^{3/2}. \quad (\text{A.14})$$

Equations (A.7), (A.8), (A.13), and (A.14) allow now to determine the normalized volume fraction as a function of annealing time.

References

- [1] J. Castaing, P. Costa, *Boron and refractory borides*, V. I. Matkovich (ed.) (1977) 390.
- [2] R. A. Cutler, *Engineering Properties of Borides* in: *Engineered Materials Handbook vol. 4*, S. J. Schneider jr. (ed.) (Metals Park, ASM International, 1991).
- [3] I. Mitra, R. Telle, *J. Solid State Chem.* 133 (1997), 25.
- [4] R. Telle, E. Fendler, E. Petzow, *J. Hard Mat.* 3 (1992), 211.
- [5] C. Schmalzried, R. Telle, B. Freitag, W. Mader, *Z. Phys.* 92 (2001), 1197.
- [6] I. Mitra, *Gefügeentwicklung und Plättchenwachstum im System der Übergangsmetallboride TiB_2 , W_2B_5 und CrB_2 zur Dispersionsverstärkung von Carbidkeramik*, PhD thesis, (RWTH Aachen, 1998).
- [7] H. Schmidt, G. Borchardt, C. Schmalzried, R. Telle, H. Baumann, S. Weber, H. Scherrer, *J. Europ. Ceram. Soc.* 23 (2003), 991.
- [8] A. N. Kolmogorov, *Bull. Acad. Sci. U.S.S.R. Phys. Ser.* 3 (1937), 555.
- [9] A. M. Johnson and R. F. Mehl, *Trans. Am. Inst. Min. Engrs* 135 (1939), 416.
- [10] M. Avrami, *J. Chem. Phys.* 7 (1940), 212.
- [11] T. Pradell, D. Crespo, N. Clavaguera, M. T. Clavaguera-Mora, *J. Phys.: Condens. Matter* 10 (1998), 3833.
- [12] J. W. Cahn, *Act. Metall.* 4 (1956), 449.
- [13] J. W. Cahn, *Act. Metall.* 5 (1957), 169.

- 1
2
3 [14] A. S. Bakai, H. Hermann, N. P. Lazarev, *Phil. Mag. A* 82 (2002), 1521.
4
5
6
7 [15] H. Schmidt, G. Borchartd, C. Schmalzried, R. Telle, S. Weber, H. Scherrer, *J. Mater.*
8
9 *Sci.*, submitted.
10
11
12 [16] J. W. Christian in: *Physical Metallurgy*, R.W. Cahn (ed.), (North Holland, Amsterdam,
13
14 1965), 443.
15
16
17
18
19
20
21
22
23
24
25
26
27
28
29
30
31
32
33
34
35
36
37
38
39
40
41
42
43
44
45
46
47
48
49
50
51
52
53
54
55
56
57
58
59
60

For Peer Review Only

Figure Captions

Figure 1: (a) XRD diagram of a homogenized $(\text{Ti}_{0.4}\text{W}_{0.5}\text{Cr}_{0.1})\text{B}_2$ sample and a sample additionally annealed at 1575 °C for 14 hours. Bragg peaks: matrix phase of type TiB_2 (○); W_2B_5 precipitation phase (●). In (b) the growth of the (004) peak of the precipitation phase is illustrated as a function of annealing time at 1500 °C. The diffractograms are shifted for clarity.

Figure 2: JMAK diagrams ($\ln(-\ln(1-X))$ vs. $\ln t$) of the precipitated volume fraction, X , at different annealing temperatures. The straight lines represent least-squares fits of equation (A.5) to the experimental data.

Figure 3: SEM micrographs of a $(\text{Ti}_{0.4}\text{W}_{0.5}\text{Cr}_{0.1})\text{B}_2$ sample annealed at 1575 °C for (a) 1 h, (b) 5 h, (c) 9 h, and (d) 14 h. The light grey regions correspond to precipitated particles, the black areas to pores, and the grey areas to the supersaturated matrix. The growth of a precipitate nucleated at a grain boundary is indicated by an arrow.

Figure 4: Square of the precipitate dimension as a function of annealing time, exemplarily shown for temperatures of 1500 and 1575 °C as obtained by image analysis of SEM micrographs. The straight lines represent least-squares fits of equation (A.8) to the experimental data.

Figure 5: Schematic sketch of particles nucleated at a grain boundary plane (x - y plane) and of an area, A_c , around a special particle (hatched). In the volume $a A_c$ atoms contribute to the growth of this particle by grain boundary diffusion, where the grain boundary width in z -direction is defined as about a .

Figure 6: Numerical calculations of (a) the precipitate fraction, X , and (b) the differential JMAK exponent, n_{diff} , as a function of annealing time according to the GBJMAK model. The following parameters are used (I) $I_B = 2 \times 10^7 \text{ m}^{-2} \text{ s}^{-1}$, $N_{B0} = 0$, (II) $I_B = 2 \times 10^7 \text{ m}^{-2} \text{ s}^{-1}$, $N_{B0} = 3 \times 10^{10} \text{ m}^{-2}$, and (III) $I_B = 2 \times 10^7 \text{ m}^{-2} \text{ s}^{-1}$, $N_{B0} = 2.5 \times 10^{11} \text{ m}^{-2}$ together with an effective diffusivity of $D_e = 1.2 \times 10^{-15} \text{ m}^2 \text{ s}^{-1}$. The dashed lines mark the region where experimental data can be obtained.

Figure 7: Numerical calculations of (a) the precipitate fraction, X , and (b) the differential JMAK exponent, n_{diff} , according to the GBJMAK model for various nucleation rates I_B with

1
2
3 $N_{B0} = 0$ and $D_e = 1.2 \times 10^{-15} \text{ m}^2 \text{ s}^{-1}$: (I) $I_B = 1 \times 10^6 \text{ m}^{-2} \text{ s}^{-1}$, (II) $I_B = 4 \times 10^6 \text{ m}^{-2} \text{ s}^{-1}$, (III) $I_B = 4$
4 $\times 10^7 \text{ m}^{-2} \text{ s}^{-1}$, and (IV) $I_B = 4 \times 10^9 \text{ m}^{-2} \text{ s}^{-1}$.
5
6

7 **Figure 8:** Experimentally derived precipitate fraction, X , at 1500 °C in comparison to
8 numerical calculations according to the GBJMAK model for different values of I_B and N_{B0} for
9 a diffusivity of $D_e = 1.2 \times 10^{-15} \text{ m}^2 \text{ s}^{-1}$.
10
11

12 **Figure 9:** (a) Experimentally derived precipitate fraction, X , as a function of annealing time
13 (symbols) in comparison to numerical calculations according to the GBJMAK model (lines)
14 at various temperatures. (b) Calculated differential JMAK exponent, n_{diff} , for the calculated
15 curves in (a).
16
17

18 **Figure 10:** Bulk diffusivities D_v , as determined from the precipitate growth curves in Fig. 4 as
19 a function of reciprocal temperature. Also shown are the tracer diffusivities of Ti obtained for
20 samples with the same chemical composition (from Ref. [15]).
21
22

23 **Figure 11:** Nucleation rates as a function of reciprocal temperature as obtained from fitting
24 the GBJMAK model to the experimental data. Also shown are the rate constants of
25 precipitation as a function of reciprocal temperature as obtained directly from the
26 experimental data. For further details see text.
27
28
29
30
31
32
33
34
35
36
37
38
39
40
41
42
43
44
45
46
47
48
49
50
51
52
53
54
55
56
57
58
59
60

Figure 1, Fotsing et al.

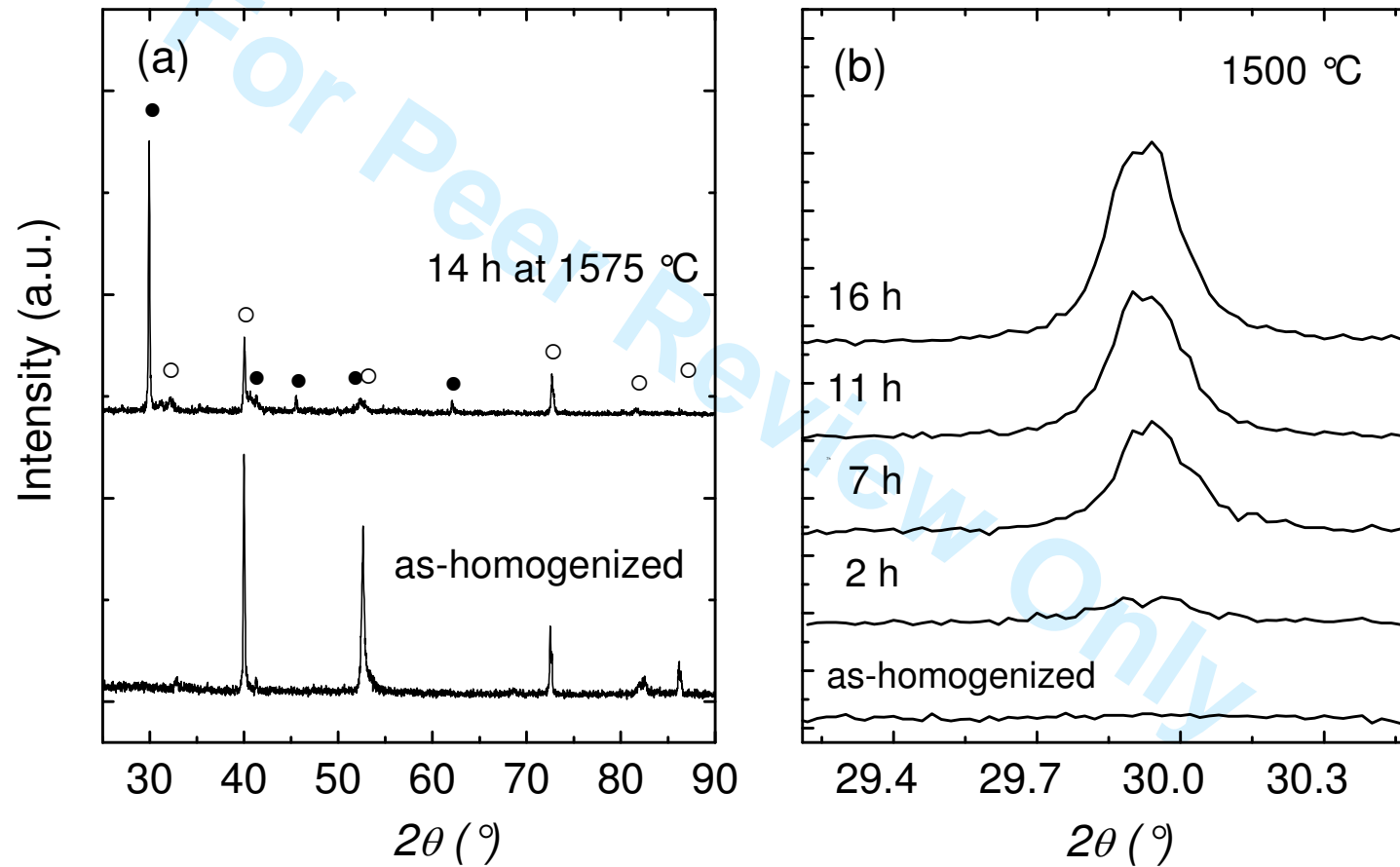


Figure 2, Fotsing et al.

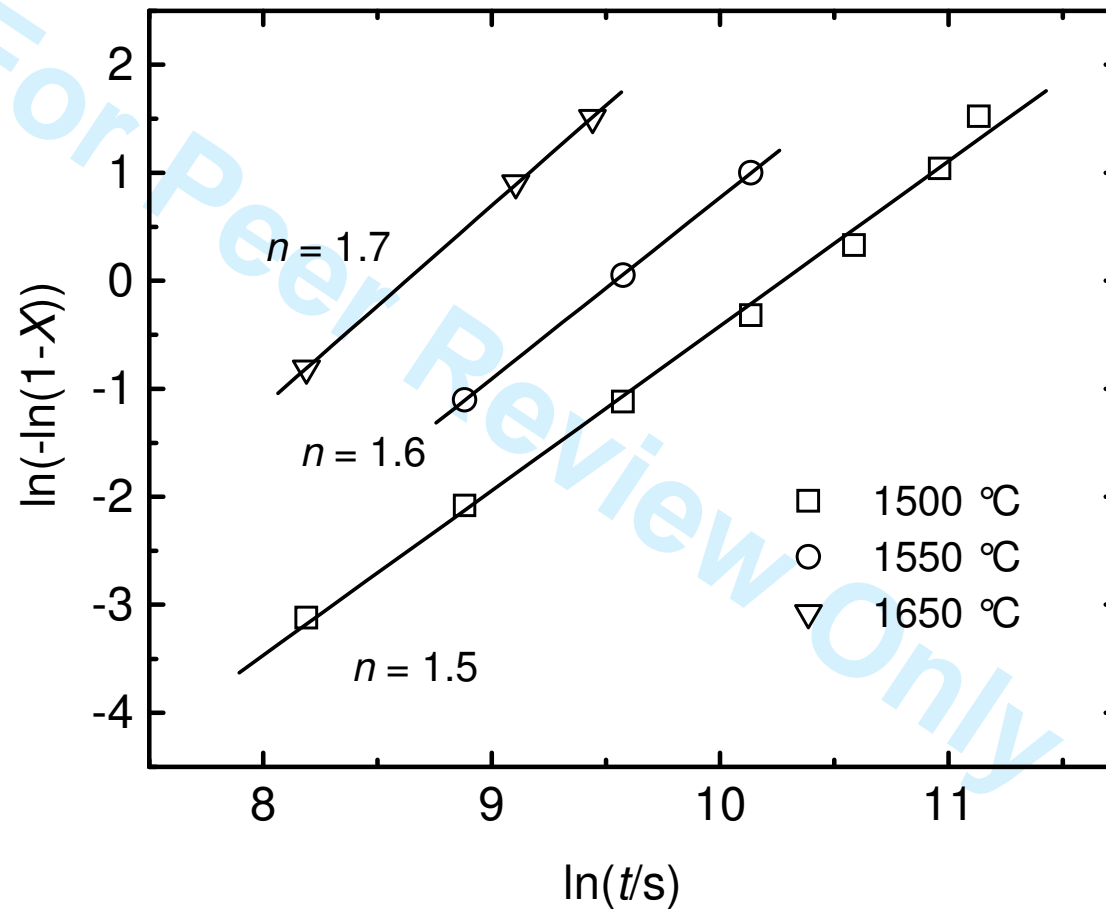


Figure 3, Fotsing et al.

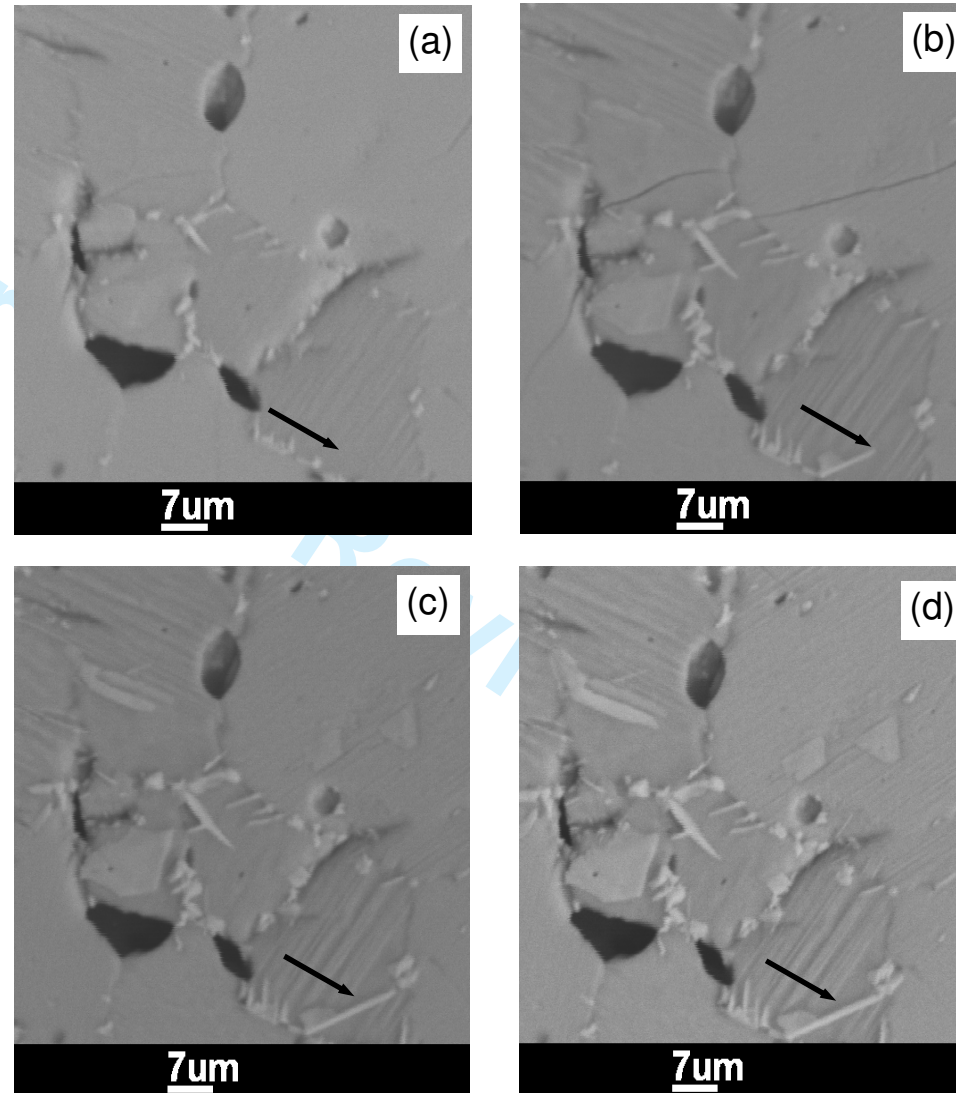


Figure 4, Fotsing et al.

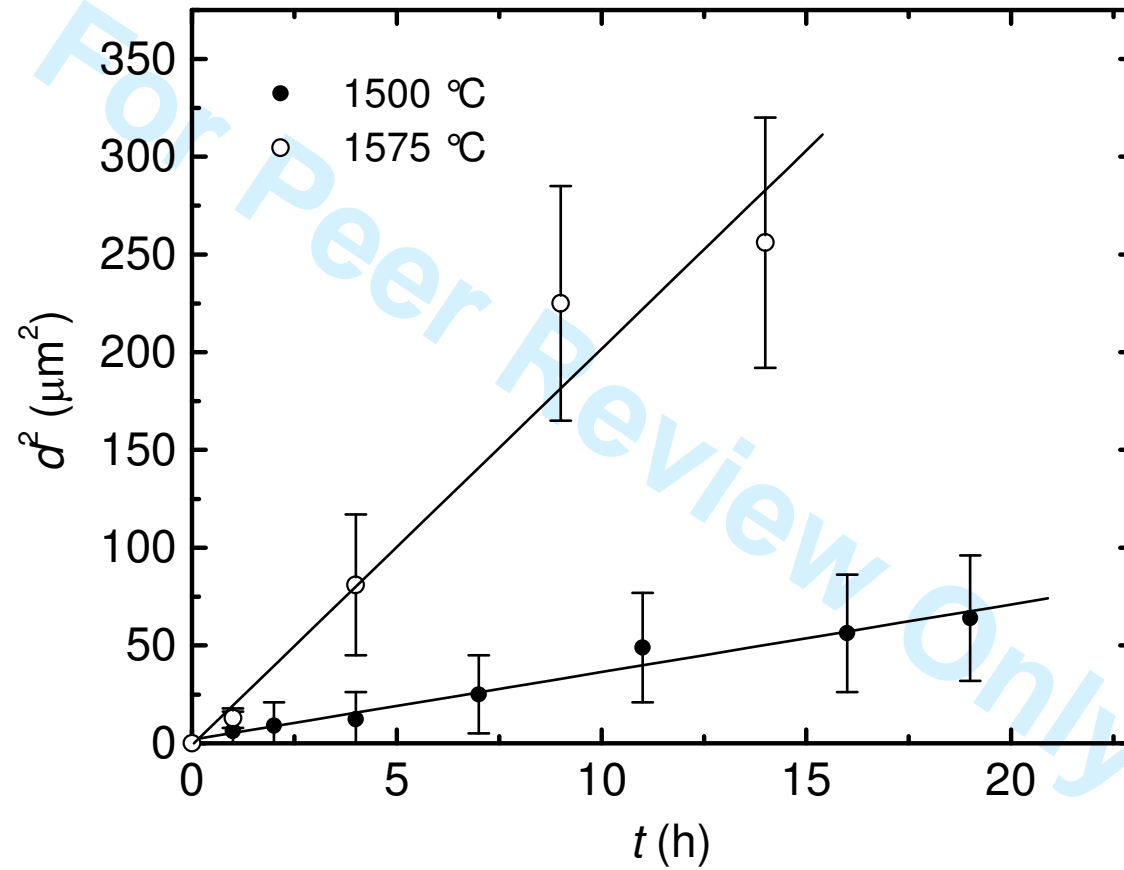


Figure 5, Fotsing et al.

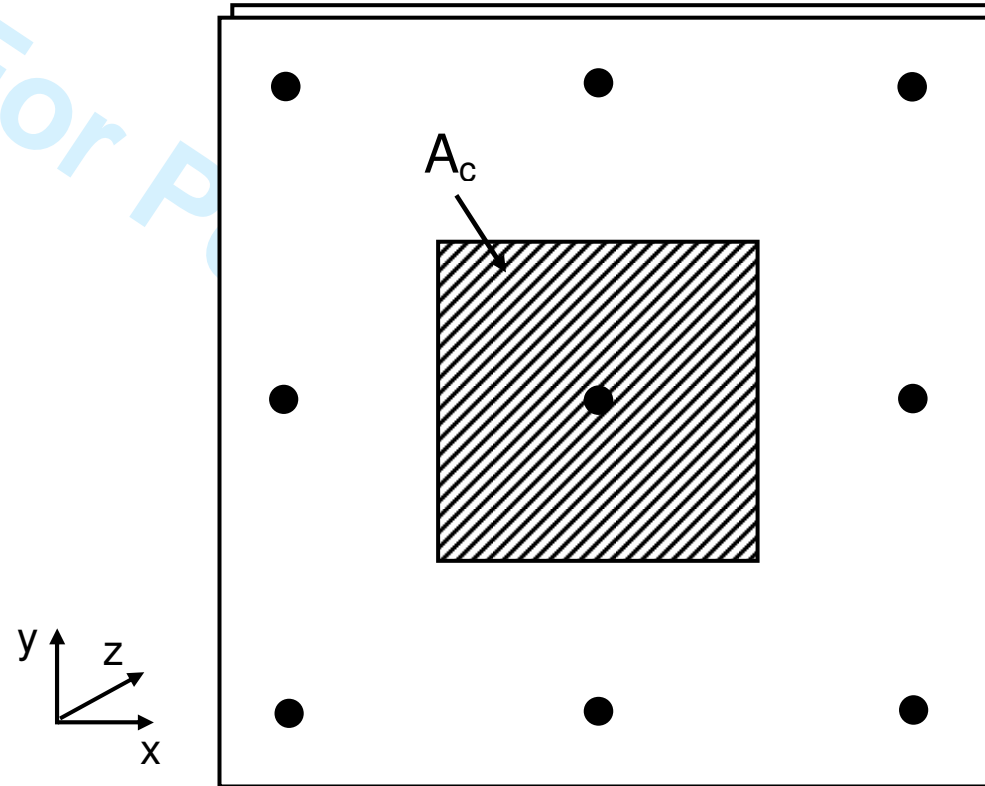


Figure 6, Fotsing et al.

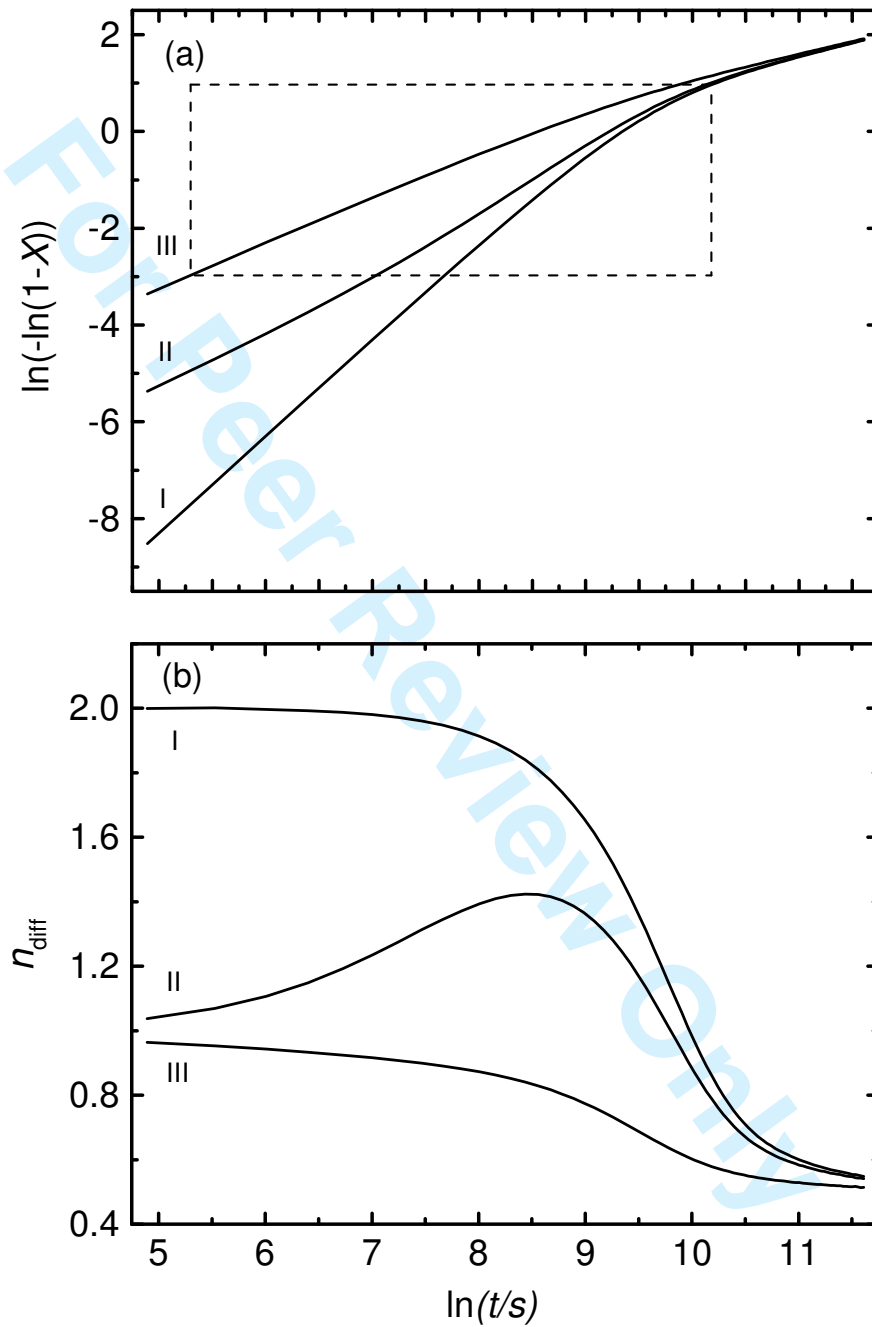


Figure 7, Fotsing et al.

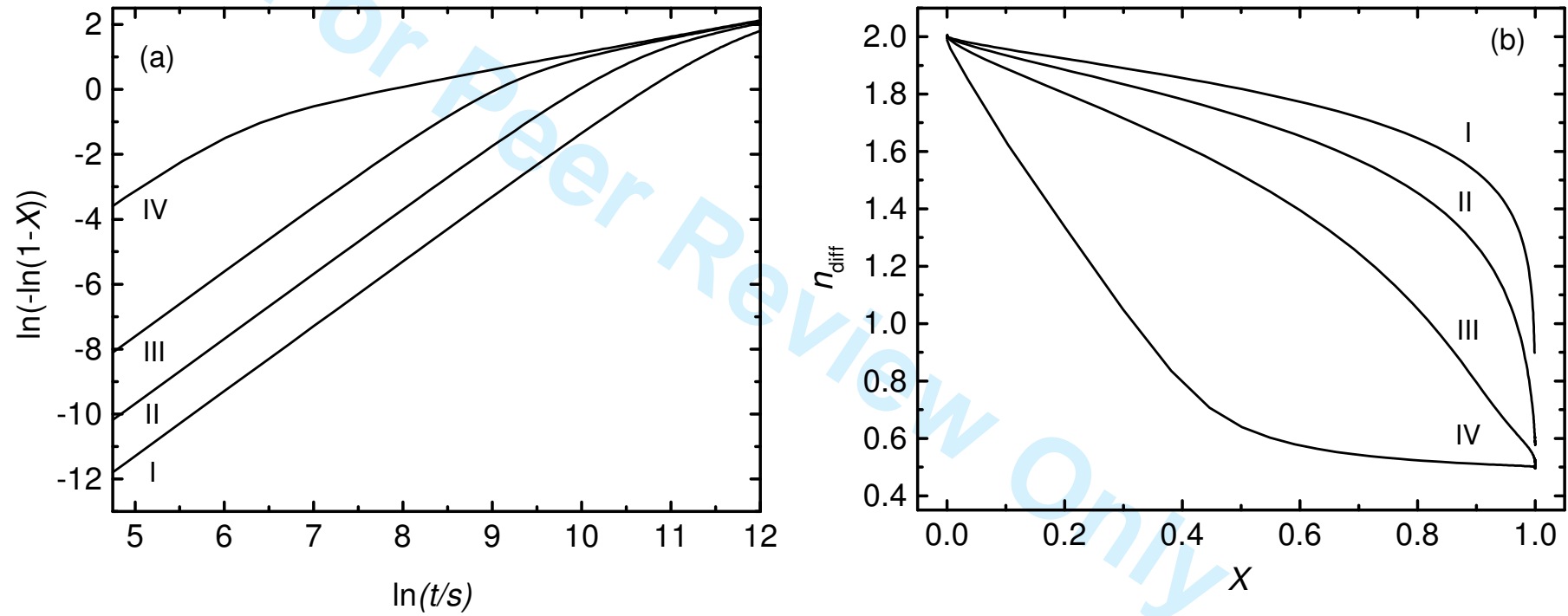


Figure 8, Fotsing et al.

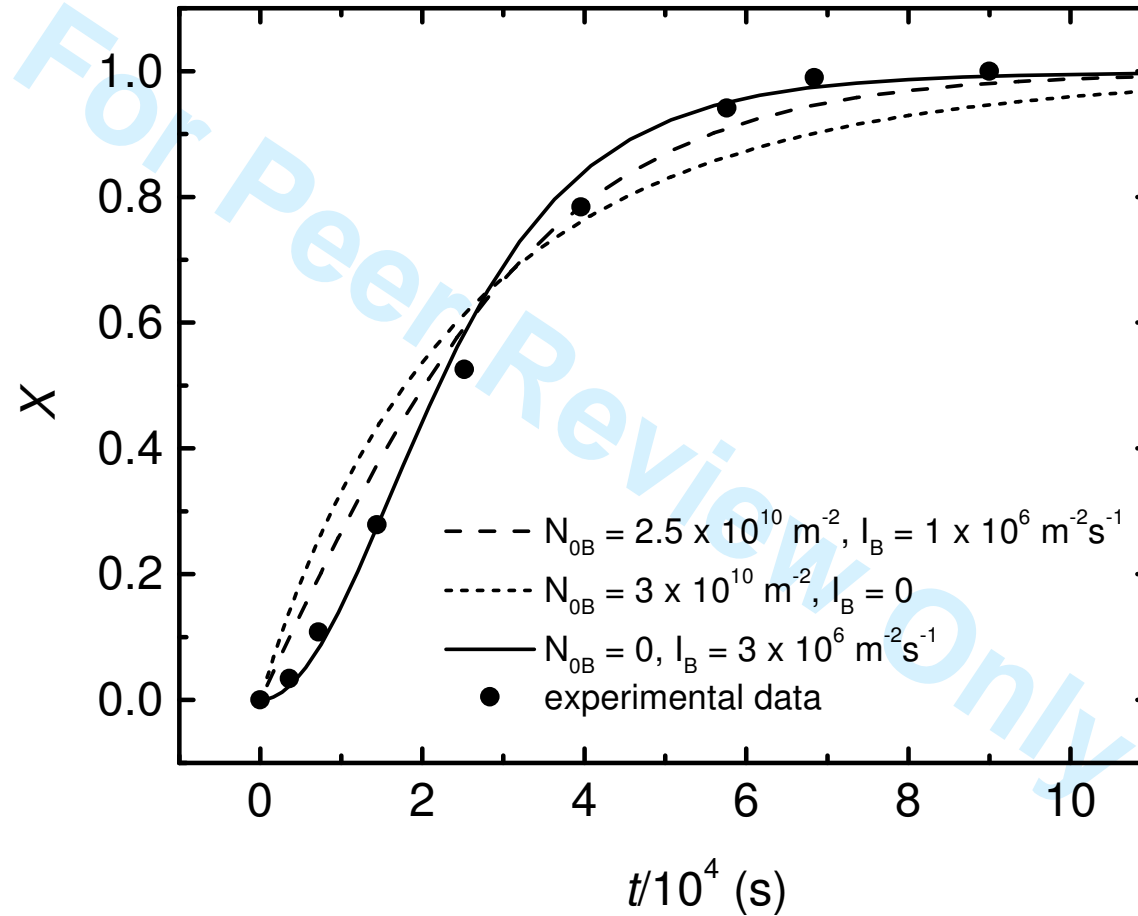


Figure 9, Fotsing et al.

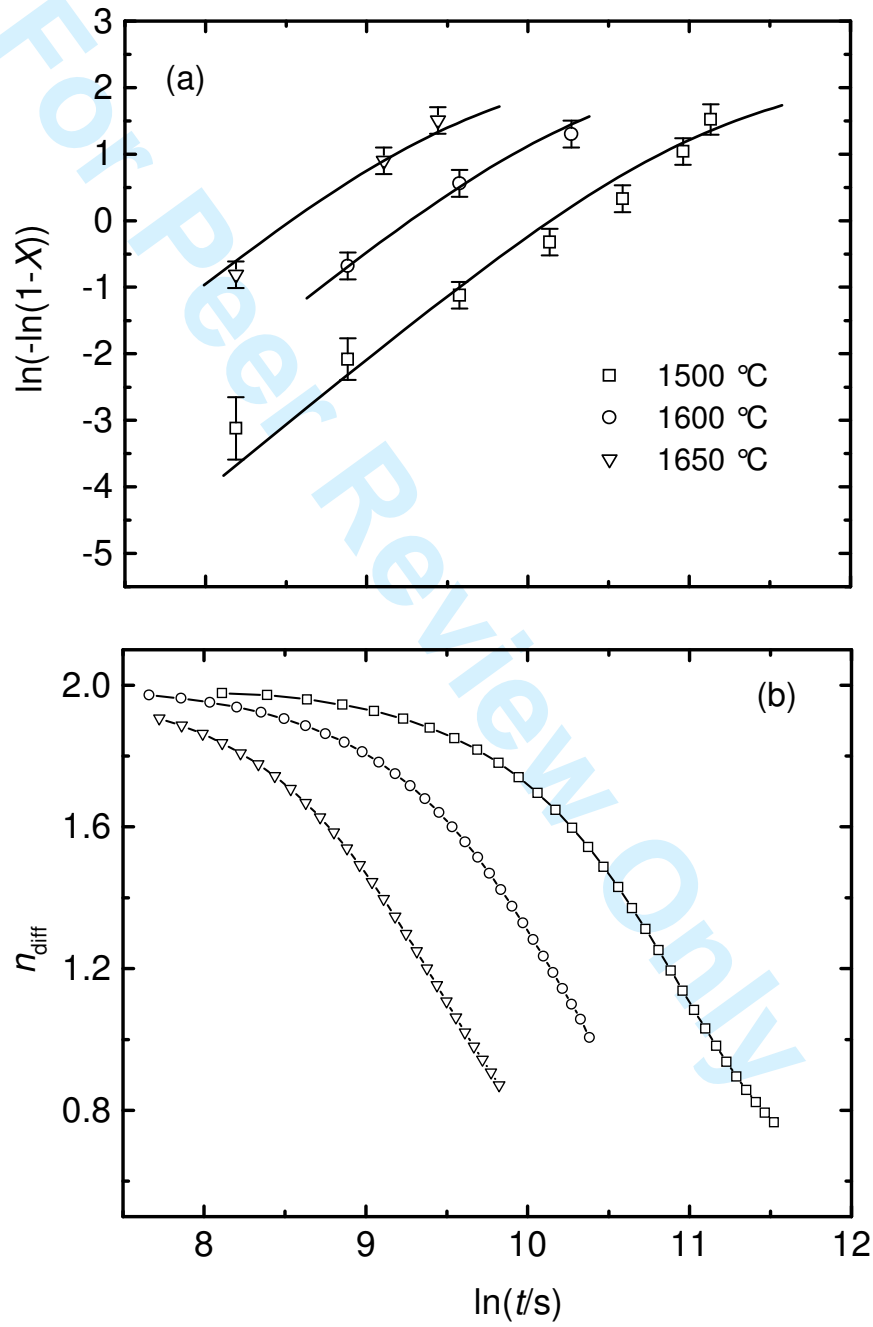


Figure 10, Fotsing et al.

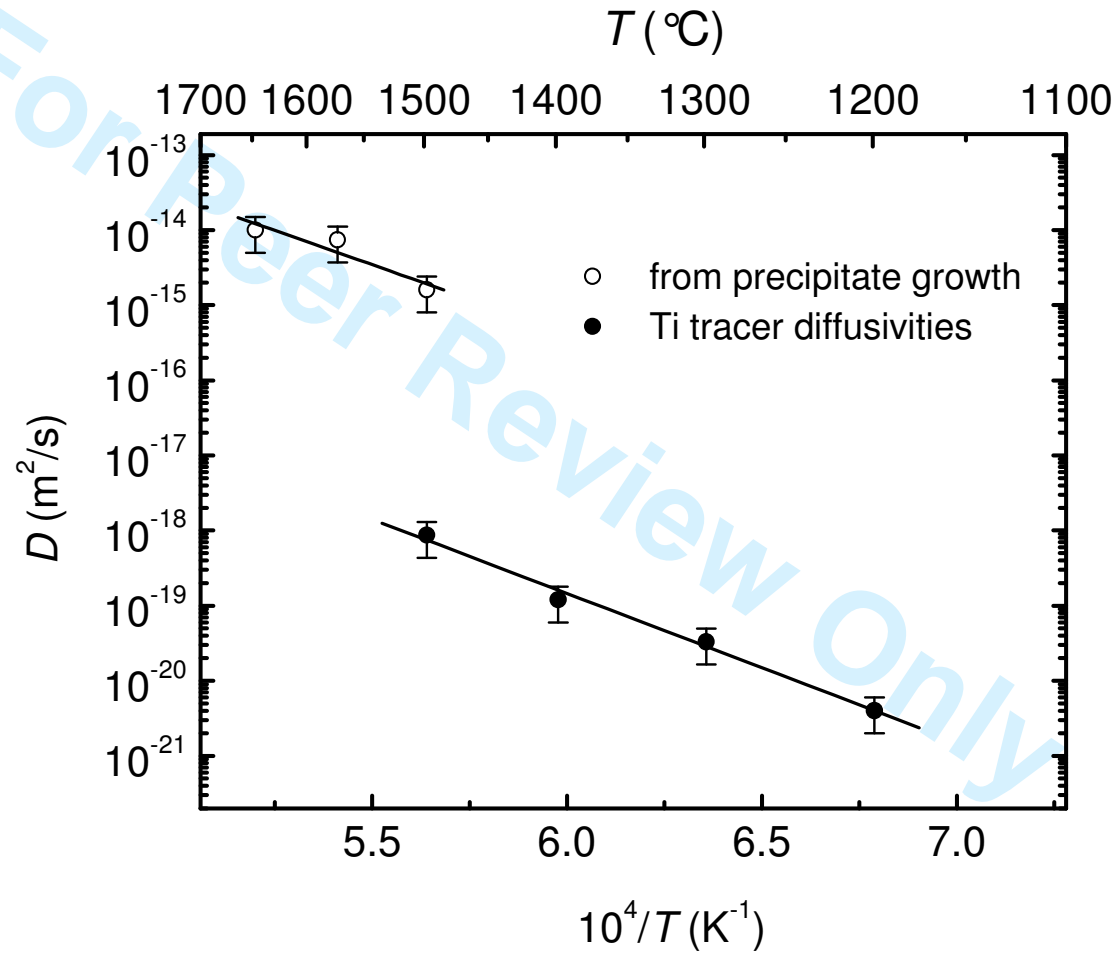


Figure 11, Fotsing et al.

